TISSUE ENGINEERING: Part A
Volume 19, Numbers 23 and 24, 2013

DOI: 10.1089/ten.tea.2012.0739

Effects of Chitosan Coatings on Polypropylene Mesh for Implantation in a Rat Abdominal Wall Model

Natasha Udpa, MS,[1] Shama R. Iyer, BS,[1] Rohit Rajoria, DVM,[2] Kate E. Breyer, DVM,[2] Helen Valentine, DVM,[2] Bhupinder Singh, DVM,[2] Sean P. McDonough, DVM, PhD,[2] Bryan N. Brown, PhD,[3] Lawrence J. Bonassar, PhD,[1,4] and Yingxin Gao, PhD[1]

Hernia repair and pelvic floor reconstruction are usually accompanied with the implantation of a surgical mesh, which frequently results in a foreign body response with associated complications. An ideal surgical mesh that allows force generation of muscle tissues without significant granulation tissue and/or fibrosis is of significant clinical interest. The objective of the present study was to evaluate the *in vitro* and *in vivo* responses of a chitosan coating on polypropylene mesh (Ch-PPM) in comparison with commercially available meshes. We found that application of a 0.5% (w/v) Ch-PPM elicited preferential attachment of myoblasts over fibroblast attachment *in vitro*. Therefore, we test the hypothesis that 0.5% Ch-PPM will encourage skeletal muscle tissue ingrowth and decrease fibrosis formation *in vivo*. We implanted 0.5% Ch-PPM, collagen-coated polypropylene mesh (Pelvitex™; C.R. Bard), and polypropylene (Avaulta Solo®; C.R. Bard) alone using a rat abdominal defect model. Force generation capacity and inflammatory response of each mesh were evaluated 2, 4, and 12 weeks post-implantation. We found that chitosan coating is associated with the restoration of functional skeletal muscle with histomorphologic characteristics that resemble native muscle and an early macrophage phenotypic response that has previously been shown to lead to more functional outcomes.

Introduction

Use of a knitted mesh is a common method indicated for mechanical reinforcement for abdominal hernia reconstruction and pelvic organ prolapse repair.[1] Recurrence of ventral hernias after open suture repair can occur with a reported frequency of 31–49% when performed without mechanical reinforcement provided by the mesh.[2] At least 29% of those who opt for surgery of pelvic organ prolapse and incontinence will require reoperation.[3] When used as a mechanical reinforcement in functional muscle repair, a synthetic mesh is intended to serve as a permanent implant, which remains in the patient for life.[4,5] A synthetic mesh, such as polypropylene mesh (PPM), is widely used due to its high strength. However, although the use of synthetic mesh materials significantly reduces recurrence rates by providing strong mechanical support to the abdominal wall or pelvic floor, commonly used synthetic polymers can sometimes elicit a strong foreign body reaction, often resulting in fibrous tissue encapsulation, erosion, or mesh degradation with high infection rates.[6,7] These common outcomes following mesh implantation can result in discomfort for the patient and, in some cases, a need for revision or removal of the implant. The complications are significant enough that Food and Drug Administration (FDA) issued warnings in 2007 and 2011 regarding the use of PPM on the pelvic floor.

Therefore, there is incentive to reduce aspects of the foreign body response, characterize the macrophage phenotype, and improve upon tissue integration after insertion of the mesh.[1,8,9] An ideal mesh for use in abdominal hernia repair and pelvic floor reconstruction would provide strength and elasticity similar to native tissues, that is, muscle tissue, as well as elicit tissue incorporation in place of fibrous tissue ingrowth and be resistant to infection.[10,11] Progressive ingrowth of fibrous tissue inhibits the integration of the implanted material within the tissue of interest and leads to a mismatch in mechanical properties with native tissue. Ideally, the mechanical properties of the neo-tissue should be strong enough to prevent recurrence, but not so strong as to reduce compliance of the abdominal wall or the vaginal tissue and cause adhesion formation or unpredicted mesh shrinkage.[12] This often results in pain or discomfort, which may require corrective surgeries due to complications, including mesh erosion and mesh exposure. Materials that preferentially promote the attachment of myoblasts over fibroblasts may elicit a less fibrotic host tissue response *in vivo*.

[1]Sibley School of Mechanical and Aerospace Engineering, Cornell University, Ithaca, New York.
[2]The College of Veterinary Medicine, Cornell University, Ithaca, New York.
[3]McGowan Institute for Regenerative Medicine, University of Pittsburgh, Pittsburgh, Pennsylvania.
[4]Department of Biomedical Engineering, Cornell University, Ithaca, New York.

Chitosan-based biomaterials may be ideal candidates for use in coating hernia and pelvic floor mesh materials. The polysaccharide chitosan has been shown to be an effective biomaterial in a broad spectrum of applications due to its unique biological properties, including nontoxicity, affinity for protein adsorption, antibacterial, hemostatic, fungistatic, and anti-tumoral properties.[13] Additionally, the physical and chemical properties of chitosan can be tailored to specific applications by relatively simple alterations of the molecular weight and deacetylation percentage.[13] Previous work has highlighted the mechanical properties[14,15] or inflammatory responses[4,14,16,17] of chitosan-based materials in abdominal wall models of small animals, however, there is no report describing the effect of chitosan-coated mesh on functional muscle tissue ingrowth. Given that hernia is induced by damages to the abdominal wall skeletal muscle, inflammatory response and tissue rebuilding to implantation of surgical mesh should include skeletal muscle ingrowth. We believe that by analyzing the skeletal muscle functionality, that is, active muscle force generation, data that are more physiologically relevant for repair can be provided.

The objective of our study is to examine the effects of chitosan coatings on PPM. We hypothesized that the chitosan coating will promote muscle tissue ingrowth and decrease the inflammatory response. Both *in vitro* and *in vivo* studies were conducted to test this hypothesis. In the *in vitro* study, 1:1 coculture of myoblasts and fibroblasts showed preferential attachment of myoblasts over fibroblasts to chitosan-coated PPM. The *in vivo* study was performed in an established rat model of abdominal wall defect repair.[18] The functional muscle response, histologic response, and macrophage phenotype of the reconstructed tissues were examined at 2, 4, and 12 weeks of postimplantation.

Materials and Methods

Overview of experimental design

All procedures were performed in accordance with the National Institute of Health (NIH) guidelines for care and use of laboratory animals, and with approval of the Institutional Animal Care and Use Committee (IACUC) at the Cornell University. The study involves both *in vitro* and *in vivo* experiments. The *in vitro* study was performed using a reference PPM (Avaulta Solo®; C.R. Bard) and different concentrations of chitosan coatings on PPM. The mesh coated with chitosan that maximized cell attachment and yielded a high myoblast to the fibroblast ingrowth ratio was selected for the *in vivo* study. In the *in vivo* portion of the study, an additional mesh was added, a monofilament PPM coated with hydrophilic porcine collagen (Pelvitex™; C.R. Bard, Inc.).

Preparation of chitosan-coated meshes and characterization

A high molecular weight chitosan, >75% deacetylated, ~600,000 MW (Sigma Aldrich) was added to distilled H_2O at concentrations of 0.3%, 0.5%, and 0.7% (w/v) and 1% (v/v) of acetic acid solution until a clear solution was obtained. The sterile PPM was cut into 1.2×1.2-cm squares and placed into a sterile bottle containing the 0.2 μm-filtered chitosan solution and stir bar. The mesh was removed from the solution, placed in a centrifuge tube, and left in liquid nitrogen for several hours, while being placed in the lyophilizer at −40°C for 24 h. The mesh was sterilized under ultraviolet light for 20 min. Scanning electron microscope (Leica 440) and Fourier transformation infrared spectroscope (FTIR; Bruker Vertex 80v) using Opus 6.0 Software were used to confirm the successful coating. PPM was also subjected to the same coating procedure minus the addition of chitosan to ensure that procedural effects to do not alter the structure of the PPM material. Pore diameters were measured from the scanning electron microscope (SEM) images using ImageJ 1.45s (NIH, 2009). A representative mesh of each Ch-coated mesh type was selected, imaged, and 10 chitosan pores were selected at random for measurement. The range was recorded.

Overview of in vitro *study*

Neonatal and adult CD-1 mice (Charles River Laboratories International, Inc.) were sacrificed for isolation of myoblasts and dermal fibroblasts, respectively. Isolation of cell types was modified from a pre-existing protocol.[19] Cells were independently passaged to four generations, stained with a long-term lipophilic tracer, and then seeded 1:1 atop one of the four different test articles: PPM, 0.3% chitosan-coated PPM (Ch-PPM), 0.5% Ch-PPM, and 0.7% Ch-PPM. The mesh samples were imaged at 12, 24, and 48 h.

In vitro *immunocytochemistry and coculture*

Isolation of myoblasts and fibroblasts from mice and appropriate cell culture media were adapted from the pre-existing protocol.[19] At Passage 4, a sample of myoblasts and a sample of fibroblasts were seeded separately on glass slides and prepped for immunocytochemistry. All staining procedures were followed according to vendor instructions (Abcam). After a DAPI stain, the primary antibodies used for antibody labeling were (1) rabbit polyclonal anti-desmin (Abcam) at 1:80 dilution for identification of myoblasts, and (2) rabbit polyclonal anti-fibroblast-specific protein-1 (Abcam) at 1:40 dilution for identification of fibroblasts. The secondary antibodies used were (1) the goat polyclonal secondary antibody to rabbit (FITC) at dilution of 1:1000, and (2) the goat polyclonal secondary antibody to mouse (TRITC) at dilution 1:1000, respectively. Plates were viewed with an inverted microscope (Olympus IX-71), and images were recorded using CellSens software. The images were overlaid, and the numbers of Desmin+/DAPI+ and FSP1+/DAPI+ cells were determined in four random quadrants per dish. If cells were determined to be >95% pure, the cells remaining in culture were stained with long-chain carbocyanines: fibroblasts were stained with DiI (Invitrogen) and myoblasts were stained with DiO (Invitrogen) following instructions provided by the vendor. Following determination of purity of the desired cell culture, myoblasts and fibroblasts were seeded onto the 1.2×1.2-cm mesh samples at a cell density of 2.4×10^5 cells/cm^2. To increase wettability, all mesh samples were soaked in media for 1 h before cell seeding.

In vitro *characterization of cell attachment on mesh*

An IX-71 Olympus microscope was used to determine the ratio of the area and number of myoblasts and fibroblasts at 12, 24, and 48 h. To image the mesh, 40× magnification was

used. Each mesh was analyzed for cell numbers and cell area. The location chosen for imaging remained consistent among all mesh samples (identical weave pattern). Images were captured highlighting the fluorescent markers for myoblasts and fibroblasts, and the cell area was determined by dividing the number of fluorescent pixels by the total number of pixels in the digital image. Total numbers of each cell type were evaluated using ImageJ 1.45s (NIH, 2009). To confirm that chitosan remained on coated mesh samples for the duration of the *in vitro* study, FTIR analysis was conducted again after 48 h of the mesh being submerged in media.

Overview of in vivo *study*

Male Wistar rats (Charles River Laboratories International, Inc.) between 250 and 450 g were randomly assigned to nine groups of six each. Each rat was subjected to a partial thickness excision of a 1.2×1.2-cm section of the ventrolateral abdominal wall musculature on either side of the linea alba. The defects were repaired with one of three test articles: Ch-PPM, collagen-coated PPM or Col-PPM (Pelvitex), and PPM alone. The animals were randomly divided into three groups after surgery for survival of 2, 4, and 12 weeks. The harvested tissues were evenly split for measurement of active muscle force by a contractile test, histological analysis, and macrophage phenotyping. Native tissue was also tested as a baseline control.

In vivo *surgical procedure*

Each rat was placed in a transparent plastic anesthesia induction chamber to administer inhalation anesthesia with 2.5% isoflurane and an oxygen flow rate of 1 L/min. The ventral abdomen was clipped from the xiphoid process to the pubis, and sterile prepped with povidone–iodine scrub and warm saline. The animal was then transferred to the surgical table with a sterile drape applied over the ventral abdomen for a surgical procedure adapted from a well-established model.[18] A 4 cm ventral midline abdominal skin incision was made, and the skin and subcutaneous tissue were separated from the underlying musculature. Bilaterally, a 1.2×1.2-cm section of the external and internal abdominal oblique layers of the ventrolateral abdominal wall was excised, while the underlying transverse abdominus and peritoneum remained intact. Different test articles were placed in the ventrolateral defects and oriented with the weave pattern perpendicular to the linea alba. The defect was repaired with a size-matched piece of the chosen test article that was randomly selected before surgery. PROLENE™ sutures (Ethicon, Inc.) were placed at each of the four corners of the test article to secure the mesh to the surrounding musculature. A MONOCRYL™ suture (Ethicon, Inc.) was used to close the skin incision. Each animal was recovered from anesthesia and returned to the housing unit. Each rat received meloxicam by subcutaneous injection on the day of surgery and for two additional days. The general health status and surgical site were monitored daily and recorded for the duration of the study.

In situ *force generation testing*

Force generation tests were included to evaluate functional muscle tissue ingrowth in neo-tissue. In the first group, the rats were anesthetized by isoflurane 2, 4, or 12 weeks after insertion of the surgical mesh, and placed on an *in situ* mounting apparatus. The skin and the underlying connective tissue were cleared from the surgical mesh placement site. The four visible PROLENE sutures, previously used to attach the surgical mesh to the partial defect, identified the surgical mesh placement site. The tests to determine the contractile property of the tissue were adapted from the protocol previously described by Valentin, *et al.*, using a muscle testing system (Aurora Scientific, Inc.).

After creating a tissue flap, to perform the testing across the muscle sections uniformly, the resting tension was set at ~2 g before testing. The tetanic force was generated at this length with electrical stimulation for 1 s at frequencies of 30, 60, 70, and 80 Hz with a rest period of 2 min following each tetanic force generation. The maximum tetanic force generation for each frequency was recorded by averaging the tetanic force generation of the muscle from 0.1 s after start of stimulation to 0.1 s before end of stimulation, subtracted by the resting tension.

Histology

In the second group, after rats were euthanized, constructs were dissected off and split into two sets, for (1) hematoxylin and eosin (H&E) staining and (2) macrophage phenotyping and myogenin expression. The first set was fixed by immersion in 10% neutral buffered formalin, embedded in glycol methacrylate, sectioned at 3 μm, and stained with H&E. A board certified veterinary pathologist (S.P.M.), who was blinded to the treatment groups, examined the H&E stained mesh constructs by light microscopy. The severity of the inflammatory response was assessed using a well-established grading scheme (Table 1) with minor modifications[20,21]: the width of the inflammatory reaction and scar was measured on a digital image of each slide created with an Aperio ScanScope microscope slide scanner. The ruler tool in the Aperio ImageScope v9.1.19 software was calibrated using a digital image of a 1 mm calibration slide (Carl Zeiss). The average width of the inflammatory reaction or scar obtained from a total of 10 sections selected at random along the length of the construct was used in the tissue reaction scoring scheme. Each sample received a scoring outcome of mild, moderate, or severe inflammatory response.

Assessment of macrophage phenotype and expression of myogenin

Macrophages have been described to have a spectrum of phenotypes, which range from classically activated and proinflammatory (M1) to alternatively activated, anti-inflammatory, regulatory and wound healing (M2). Using the second set of the mesh used for histology purposes, the phenotype of macrophages responding to each mesh material were assessed as previously described[8] after embedding in paraffin. Briefly, histologic sections were dewaxed through immersion in xylenes and a graded series of ethanol (100–70%). Antigen retrieval was then performed by immersion in 10 mM citric acid monohydrate (pH 6.0) at 95°C for 20 min. The slides were allowed to cool and were then washed in TRIS buffered saline/Tween 20 solution (pH 7.4) and PBS. The sections were then blocked in 2% normal horse

Table 1. Method of Semiquantitative Histopathological Assessment

1. Tissue reaction scoring

Tissue reaction element	*Grading factor × weight factor = score*
Width of inflammation[a]	5
Width of scar[a]	1
Overall density of cellular reaction[b]	5
Number of cells[a]	
Neutrophils	6
Lymphocytes	2
Plasma cells	2
Eosinophils	1
Macrophages	1
Giant cells	1
Fibroblasts	1
Total score	

2. Tissue reaction grade

Total score	*Tissue reaction grade*	*Designation*
1–10	1	Minimal
11–25	2	Mild
26–40	3	Moderate
>40	4	Severe

a. Width of inflammation or scar (diameter of response in μm)	*No. cells (per 60×field)*	*Grade*
0	0	0
1–200	1–50	1
201–400	51–100	2
401–600	101–200	3
>600	>200	4

b. Overall density of cellular reaction (assignment based on experience of pathologist)	
Bare scattering	1
	2
	3
Dense aggregation	4

serum, 1% BSA, 0.1% Triton X-100, and 0.1% Tween 20 in PBS (pH 7.4) for 1 h at room temperature. The sections were then exposed to antibodies specific for a pan-macrophage (M0) marker (1:50, mouse anti-CD68; Serotec), a M1 phenotype marker (1:50, rabbit anti-CD86; Abcam), and an M2 phenotype marker (1:50, goat anti-CD206; Santa Cruz) overnight at 4°C. The slides were washed in PBS and then incubated in appropriate secondary antibodies. The secondary antibodies used were Alexa Fluor donkey anti-mouse IgG (594 nm, 1:150; Life Technologies), Alexa Fluor donkey anti-goat IgG (488 nm, 1:150; Life Technologies), and donkey anti-rabbit IgG PerCP 5.5 (1:200; Santa Cruz). The slides were then coverslipped with aqueous mounting media containing DAPI. Representative sections from each sample group at the 14-day time point were examined and imaged by a blinded investigator using a Nikon e600 microscope equipped with a Nuance multispectral imaging system.

Myogenin is a part of the myogenic regulatory gene family, which includes MyoD, myf5, and MRF4. These genes encode a set of transcription factors that are essential for muscle development. Expression of myogenin is limited to cells of skeletal muscle origin.[22] Additional sections were taken from the paraffin-embedded blocks used for macrophage phenotypes. These sections were stained with monoclonal mouse anti-myogenin clone F5D (Dako North America, Inc.). All staining procedures were followed according to vendor instructions. Representative sections from each sample group were imaged at the 14-day time point.

Statistical analysis

For *in vitro* results in Figure 3A, statistical significance ($p < 0.01$) was calculated using a two-way analysis of variance (ANOVA) with mesh, time, and their interaction term as independent variables. Mesh and time and their interaction term as independent variables. The interaction term was significant [$F(6,24) = 21.67$, $n = 3$, $p < 0.001$]. Differences between mesh samples at different time points were analyzed using a Tukey's honestly significant different (HSD) *post hoc* comparison (JMP, v.9). All values are expressed as the least mean square mean ± standard deviation.

For Figure 3B, statistical significance ($p < 0.05$) was calculated using a two-way ANOVA with mesh and time and their interaction term as independent variables. Differences between mesh samples at different time points were analyzed using the Tukey's HSD *post hoc* comparison. The analysis was done on a log-transformed dependent variable. The interaction term was significant [$F(3,16) = 23.36$, $p = 0.0027$]. Differences between mesh samples at different time points were analyzed using the Tukey's HSD *post hoc* comparison with a Bonferroni correction for multiple comparisons. All values are expressed as the least mean square mean ± standard deviation.

For *in vivo* results, in Figure 4, data were analyzed with JMP using a mixed model with random effect being the rat ID and the fixed effects being the mesh type. Both time and the interaction term of time and mesh type were independent variables. Statistical analysis was done using a mixed model with the Tukey's HSD *post hoc* comparison ($n = 4$, $p < 0.05$). Dashed line denotes force generation of native muscle tissue. All values are expressed as the least mean square mean ± standard error.

Results

Analysis of mesh materials by SEM and FTIR

Figure 1 shows the microarchitecture of the mesh materials as observed under SEM. The polysaccharide was distributed within the interstices of the mesh fibers for the Ch-PPM samples. The chitosan microarchitecture differed between 0.3%, 0.5%, and 0.7% Ch-PPM. The chitosan pore size of the different mesh samples varied. PPM has mesh pore sizes that measured 2.0 × 1.7 mm, the 0.3%, 0.5%, and 0.7% Ch-PPM has chitosan pore diameters within the polypropylene interstices that ranged from 200 μm–1.7 mm, 80–140 μm, and 10–60 μm, respectively.

As seen in Figure 2, the PPM exhibits peaks at 1375 cm^{-1} and 1450 cm^{-1} representing the alkane groups, and at

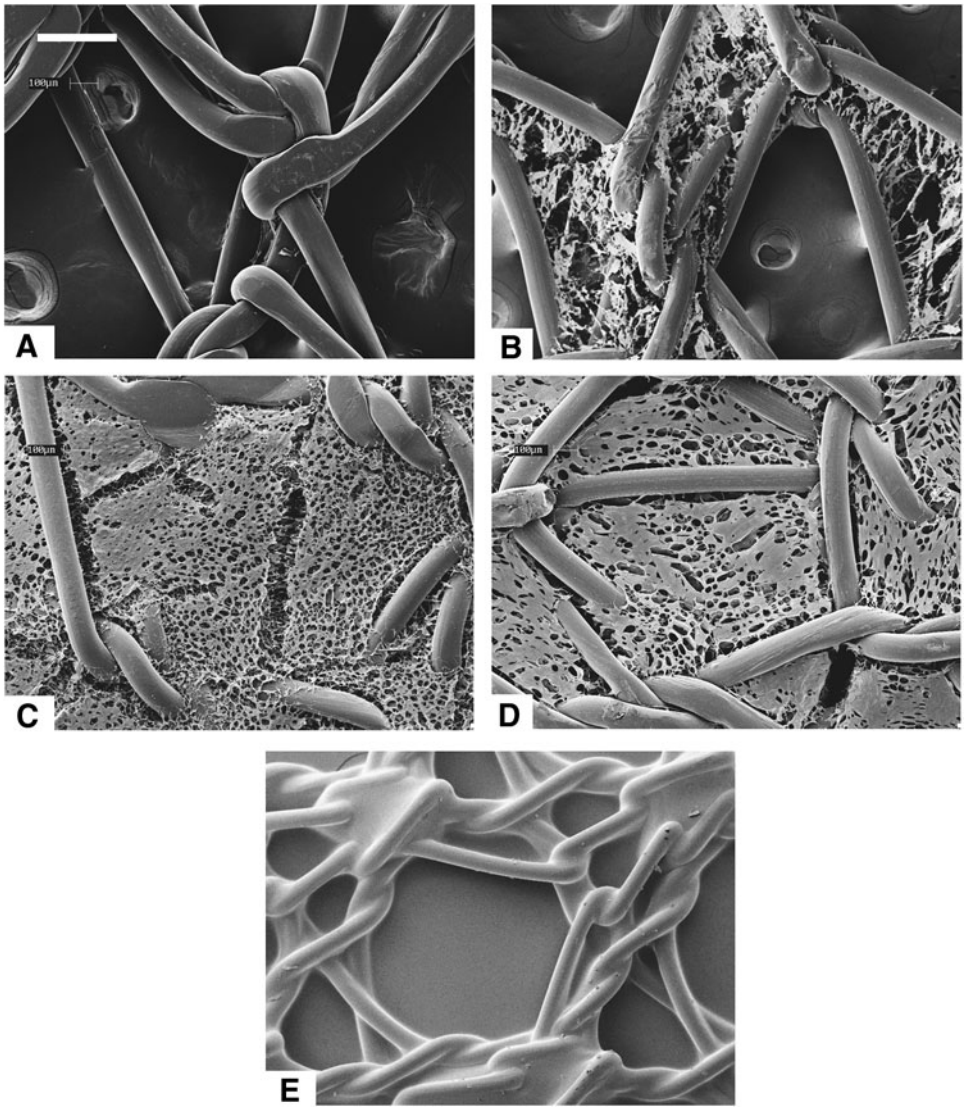

FIG. 1. Scanning electron microscope (SEM) micrographs of mesh types **(A)** Avaulta Solo® C.R. Bard, knitted polypropylene mesh (PPM), **(B)** 0.3% Ch-PPM, **(C)** 0.5% Ch-PPM, **(D)** 0.7% Ch-PPM, **(E)** Pelvitex™, C.R. bard, collagen-coated polypropylene mesh (Col-PPM). Scale bar = 300 μm. Ch-PPM, chitosan-coated PPM.

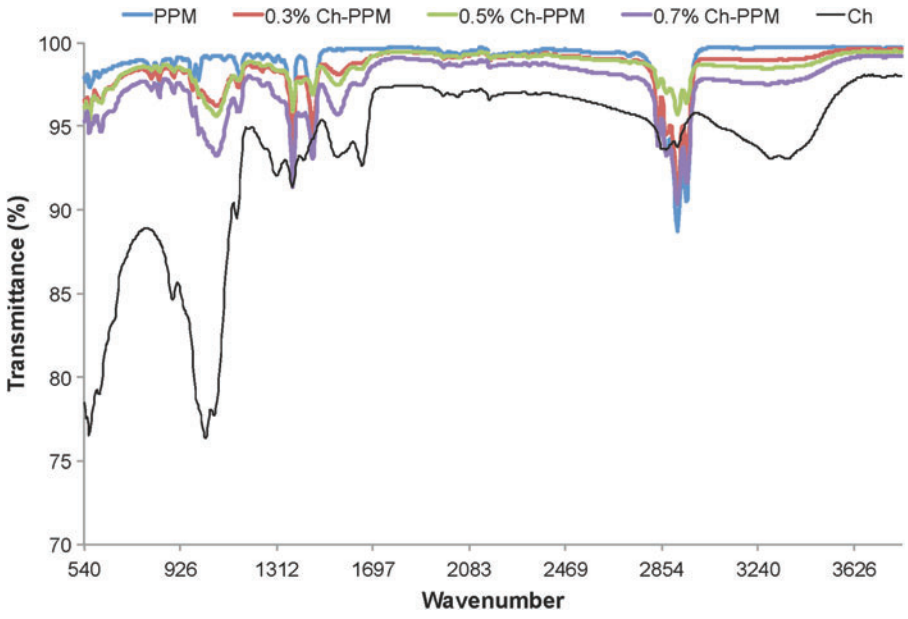

FIG. 2. FTIR spectra of high molecular weight chitosan (600,000 MW) and uncoated PPM, 0.3% Ch-PPM, 0.5% Ch-PPM, 0.7% Ch-PPM. FTIR, Fourier transformation infrared spectroscopy. Color images available online at www.liebertpub.com/tea

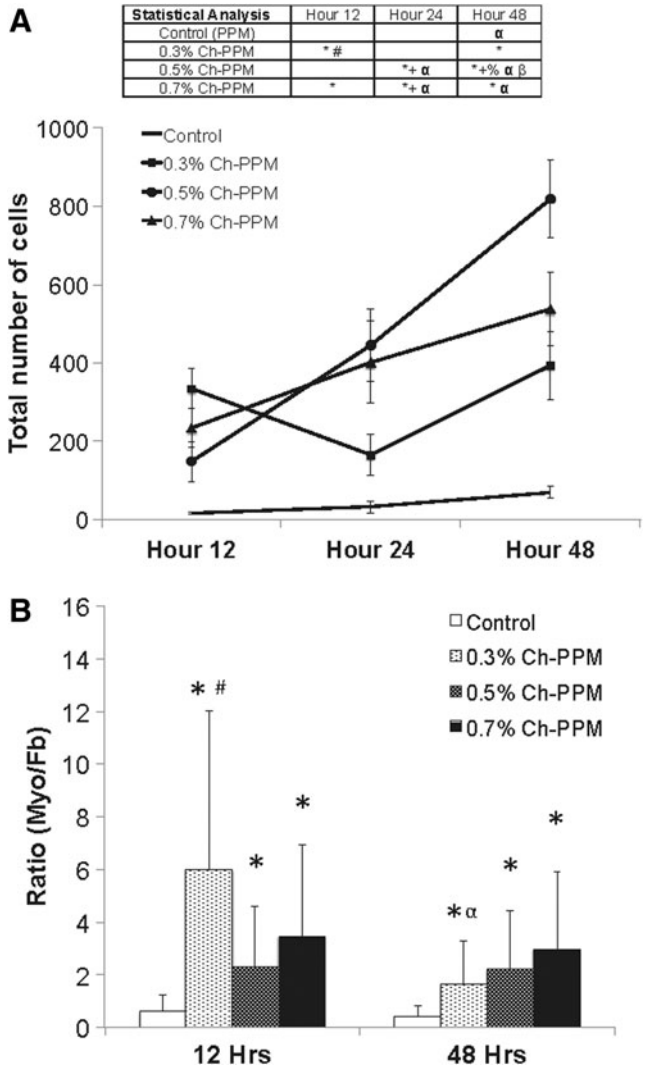

FIG. 3. **(A)** Total number of cells attached to mesh samples. "*" indicates significantly from control within time point, "+" indicates significantly different from 0.3% Ch-PPM within time point, "#" indicates significantly different from 0.5% Ch-PPM within time point, "%" indicates significantly different from 0.7% within time point, "α" indicates significantly different from 12-h time point within the same mesh type, and "β" indicates significantly different from 24-h time point within the same mesh type. **(B)** The ratio of myoblast:fibroblast (myo:fb) for mesh samples. The ratio was measured using the DiO:DiI fluorescence ratio. "*" indicates significantly different from control within time point, "#" indicates significantly different from 0.5% Ch-PPM within time point, and "α" indicates significantly different from 12-h time point within the same mesh type.

2600–3000 cm^{-1} representing the methylene and methyl groups. FTIR spectra of the Ch-PPM samples depict characteristic absorption bands at 1089, 1600–1750, and 3370 cm^{-1}, which represent glycosidic bonds, residual carbonyl groups, and the stretching vibration of the NH_2 and OH groups, respectively. These peaks were seen to increase with increasing chitosan concentrations. The FTIR after 48 h results showed that (1) after 48 h, there is still chitosan attached to the mesh, and (2) the coating procedure does not affect the

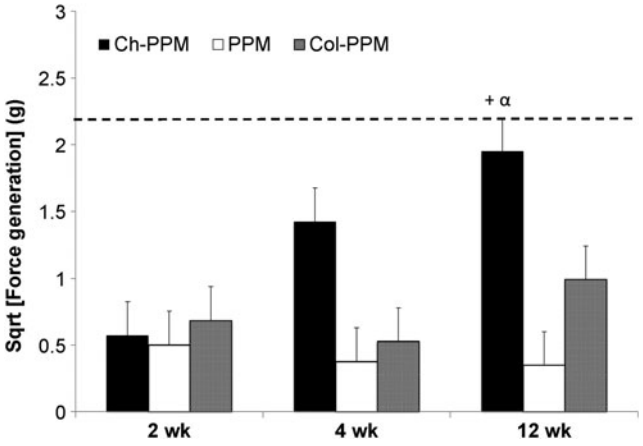

FIG. 4. *In situ* force generation of mesh samples. Dashed line indicates force generation of native tissue. "+" indicates significantly different from 12-week PPM within time point, "α" indicates significantly different from 2-week Ch-PPM.

structure of PPM material. These two observations lead us to believe that the higher myoblast to fibroblast ratio is due to the chitosan coating.

Characterization of cell attachment on mesh using fluorescent microscopy

The ratio of myoblasts to fibroblasts on the surface of cell-seeded mesh materials was measured using a pixel count of the DiO:DiI, respectively. By day 2, the total number of cells was significantly greater for all three Ch-PPMs than for the reference mesh (Fig. 3A). The ratio of myoblasts to fibroblasts for 0.3%, 0.5%, and 0.7% Ch-PPM consistently remained

Table 2. Mean Rounded Scores, Width of Inflammatory Response, and Width of Fibrosis for Each Implant[a]

Mesh (weeks)	*Average tissue reaction score*[b]	*Average width of inflammatory response [μm ± (1 SD)]*	*Average width of fibrotic response [μm ± (1 SD)]*
Ch-PPM			
2	34 (5.0)	657 (323.1)	269 (86.3)
4	32 (11.4)	162 (137.3)	440 (183.2)
12	35 (3.3)	426 (137.9)	122 (40.9)
PPM			
2	33 (0)	575 (36.8)	185 (2.8)
4	31 (7.8)	174 (167.0)	461 (129.1)
12	45 (11.1)	535 (245.9)	235 (179.60)
Col-PPM			
2	43 (10.1)	1150 (1149.5)	1468 (856.5)
4	27 (5.0)	57 (19.9)	272 (104.3)
12	46 (12.5)	549 (181.8)	143 (40.6)

[a]Scores, width of the inflammatory reaction and the width of the fibrotic response (scar) for each time point were averaged and the mean rounded to obtain the final result (one SD).

[b]Tissue reaction scores.

0 = normal; 1–10 = minimal; 11–25 = mild; 26–40 = moderate; >40 = severe.

Ch-PPM, chitosan coating on a polypropylene mesh; SD, standard deviation.

greater than 1 (Fig. 3B), indicating a higher number of attached myoblasts in comparison with fibroblasts both within the mesh interstices and atop the polypropylene fibers. The control material had a ratio of less than 1, suggesting more fibroblasts attached than myoblasts.

Statistical analysis of the same mesh across the three different time points was completed to analyze the proliferation of cells from 12 to 48 h. 0.5% Ch-PPM at 48 h was significantly different from the number of cells that attached to the same mesh at both 12 and 24 h. The number of cells that attached to 0.5% Ch-PPM at 24 h was significantly different from the cells that attached at 12 h. 0.5% Ch-PPM was the only mesh to show a significant difference across the three time points. As a result, 0.5% Ch-PPM was selected for the *in vivo* portion of the study.

Analysis of force generation

No significant differences were present among the different meshes after 2 weeks and 4 weeks of implantation (Fig. 4). After 12 weeks of implantation, 0.5% Ch-PPM had a significantly higher tetanic force response at a stimulation frequency of 60 Hz than PPM. PPM showed a negligible contractile response at 12 weeks, while Ch-PPM approached native tissue better than the PPM and in terms of tetanic response at 12 weeks. Furthermore, the contractile response of 0.5% Ch-PPM significantly increased between 2 and 12 weeks, whereas there was no significant difference between PPM and Col-PPM.

Histopathological assessment

Table 2 summarizes the histopathological assessment of the mesh samples after implantation in the abdominal wall. At 2 weeks of postimplantation, the semiquantitative histopathological assessment for the degree and type of cellular infiltrate was moderate for all meshes. The tissue reaction score for the Ch-PPM remained unchanged up to 12 weeks. In contrast, the average tissue reaction scores for both the PPM and the Col-PPM increased at 12 weeks. Although the average tissue reaction score for the Ch-PPM (35 ± 3.3) was not statistically significantly different from that of the PPM ($p = 0.08$) or the Col-PPM ($p = 0.09$), a clear trend was evident with a less intense tissue reaction induced by the Ch-PPM

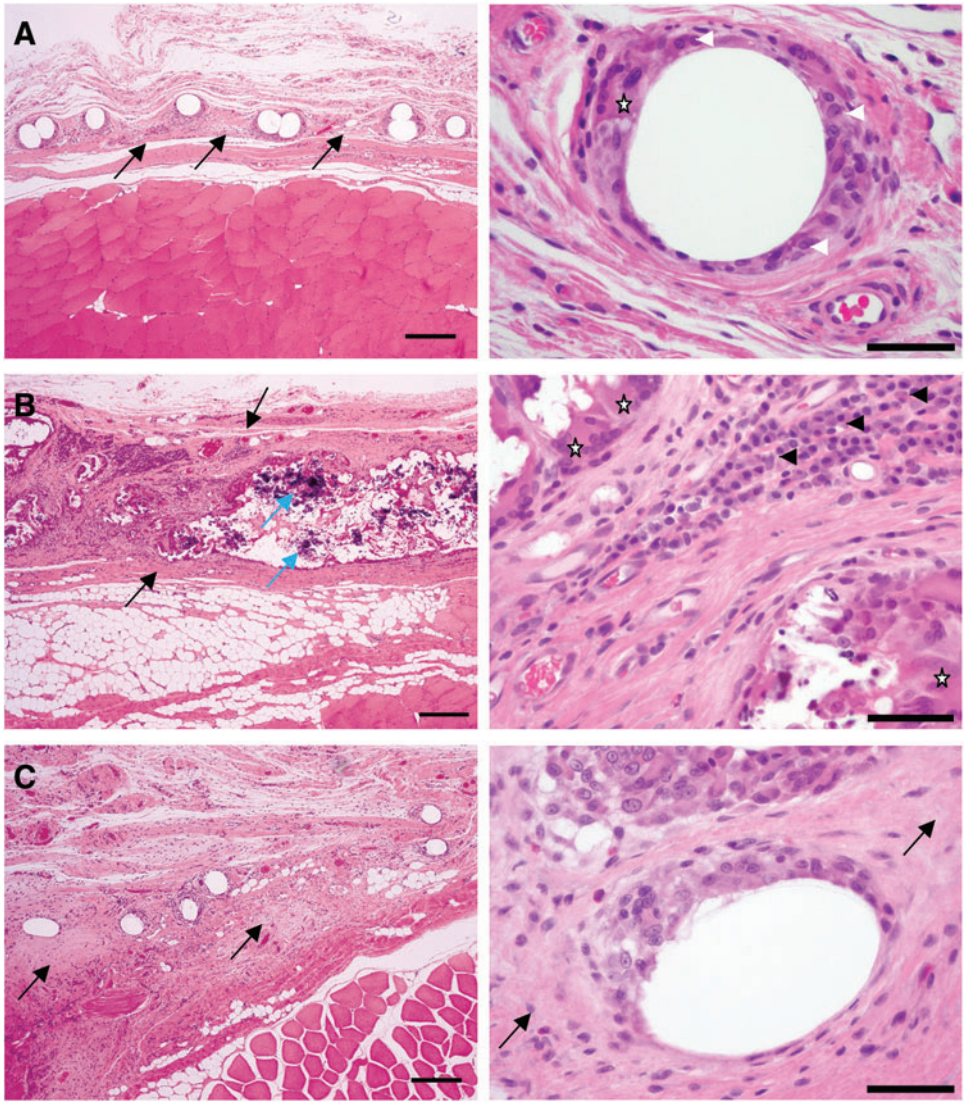

FIG. 5. Comparison of representative tissue reactions to three test mesh articles at 12 weeks of postimplantation. **(A)** Ch-PPM. **(B)** PPM (Avaulta Solo, C.R. Bard, Inc.). **(C)** Col-PPM (Pelvitex; C.R. Bard, Inc.). Ch-PPM **(A)** is embedded in a narrow band of fibrous connective tissue (black arrows) and the individual fibers are cuffed by a moderate number of macrophages (white arrow heads) and multinucleate giant cells (star). In contrast, the PPM has invoked a severe inflammatory reaction and a wide band of fibrosis (between black arrows) with large foci of dystrophic mineralization (blue arrows). Note the large clusters of plasma cells (black arrow heads) and the numerous multinucleate giant cells (stars). The Col-PPM **(C)** is embedded in a wider band of fibrosis compared to the Ch-PPM (black arrows), but only a few inflammatory cells are present. All images in the left hand column taken at $4\times$ magnification; scale bar = 500 μm. All images in the right hand column taken at $40\times$ magnification; scale bar = 50 μm. Color images available online at www.liebertpub.com/tea

(Fig. 5A). Strikingly, PPM at 12 weeks was accompanied by locally extensive areas of dystrophic mineralization (Fig. 5B, C). No dystrophic mineralization was detected around any of the Ch-PPM. The PPM was infiltrated by a large population of mixed mononuclear cells (Fig. 5B). In contrast, the inflammatory infiltrate around the Col-PPM was similar to that around the Ch-PPM, but with a moderately greater fibrotic response (Fig. 5C). Figure 6 illustrates the stable tissue reaction to the Ch-PPM at 2, 4, and 12 weeks of postimplantation.

Macrophage phenotype and expression of myogenin

Immunolabeling of representative sections from each sample group at 14 days of postimplantation revealed qualitative differences in the phenotype of the cells at the interface with the mesh material (Fig. 7). All samples were associated with a similarly intense infiltration of CD68+ macrophages at 14 days. Both the PPM and Col-PPM groups were characterized by a predominance of CD86+ (M1 marker) cells both at the surface of the mesh and between mesh fibers. The Ch-PPM group was characterized by qualitatively fewer CD86+ cells at the mesh surface and peripheral to mesh fibers. The PPM and Col-PPM samples were characterized by few CD206+ (M2 marker) cells at the mesh surface or between mesh fibers. The Ch-PPM group was characterized by the presence of CD206+ cells both at the mesh surface and peripheral to the mesh fibers.

In Figure 8, immunolabeling of representative sections from each sample mesh type at 14 days of postimplantation revealed qualitative differences in myogenin expression at the interface with the mesh material. Of the three mesh types, only the tissue samples with Ch-PPM were characterized with myogenin expression between mesh fibers. Expression of myogenin is limited to cells of skeletal muscle origin.

Discussion

Implantable mesh materials for abdominal wall repair and pelvic organ repair should provide mechanical support and allow ingrowth of the surrounding tissues. In hernia and gynecological surgery, integration of muscle tissue into the mesh is desired to accommodate the natural contractility of the muscle on the abdominal wall or the smooth muscle in

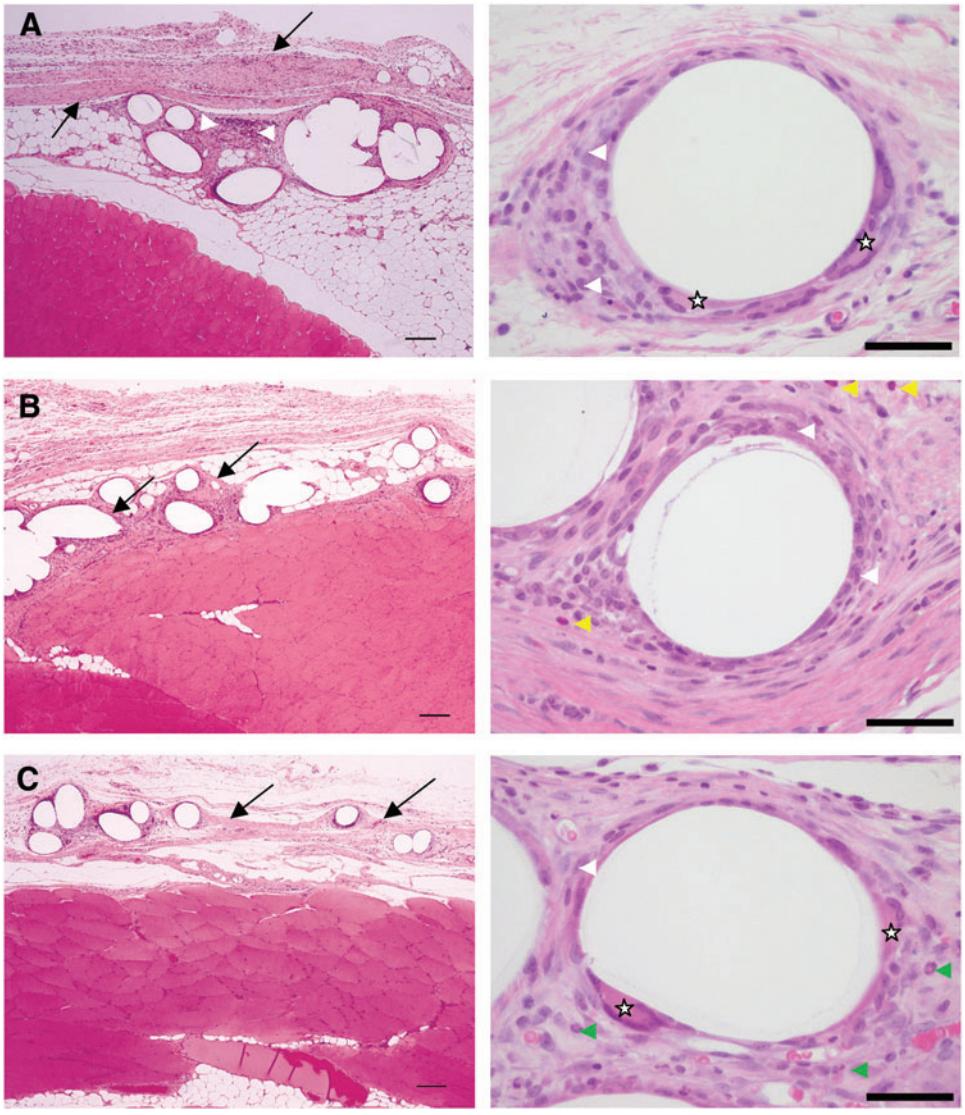

FIG. 6. Tissue reaction over time to Ch-PPM. At 2 weeks **(A)** a thin layer of fibrosis (black arrows) and mixed inflammatory cells (white arrow heads), including neutrophils (green arrow heads), eosinophils (yellow arrow heads), macrophages (white arrow heads), and multinucleate giant cells (stars) surround the mesh. The degree of fibrosis is similar at 4 weeks **(B)** and 12 weeks **(C)**, but the number of inflammatory cells is decreased and consists almost entirely of macrophages with rare multinucleate giant cells. Color images available online at www.liebertpub.com/tea

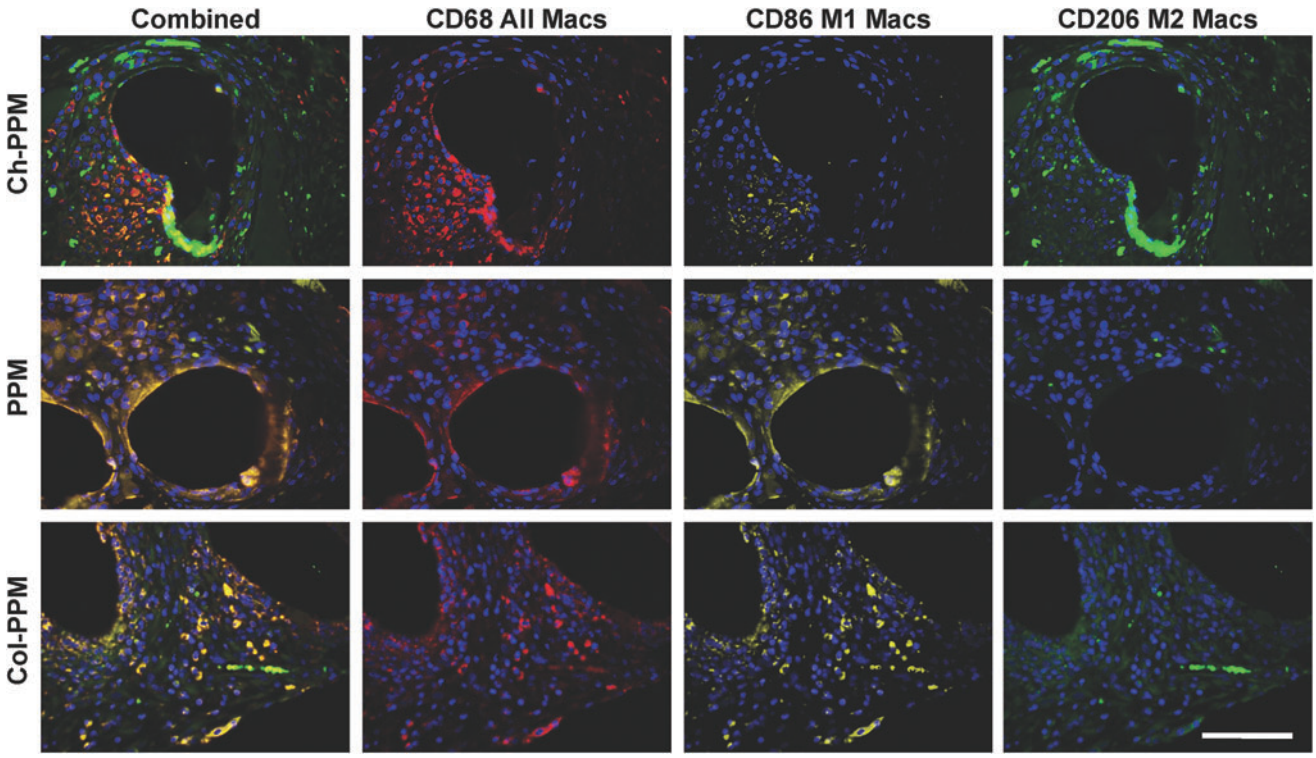

FIG. 7. Immunolabeling of macrophage surface markers. Mesh materials were labeled with a pan macrophage marker (CD68, red), an M1 marker (CD86, yellow), and an M2 marker (CD206, green). All images taken at 40×magnification. Scale bar = 100 μm. Color images available online at www.liebertpub.com/tea

the vagina. It has been shown that the strength of PPM is advantageous in abdominal wall implantation.[23] However, after implantation of the mesh, substantial fibrosis and little or no functional muscle ingrowth is commonly observed around the abdominal wall and/or the vaginal wall, despite providing adequate mechanical strength at the time of implantation. This causes significant differences in the material properties at the mesh–native tissue interface, which could result in stress concentrations and stress shielding effects, leading to mesh erosion.

The objective of our study was to examine chitosan coatings on PPM to evaluate muscle tissue ingrowth and the inflammatory response. We hypothesized that chitosan coating will promote muscle tissue ingrowth and decrease the inflammatory response. To test our hypothesis, an *in vitro* study was performed to determine the response of myoblasts and fibroblasts to different concentrations of chitosan coated on PPM. The *in vitro* results showed that the Ch-coating on PPM promotes myoblast and inhibits fibroblast attachment to the mesh. The *in vivo* study was then performed to further demonstrate that chitosan coating decreases inflammatory responses, promotes muscle tissue ingrowth, and reduces fibrosis.

Polypropylene and various concentrations of chitosan were studied *in vitro* after myoblasts and fibroblasts were seeded 1:1, which mimics the *in vivo* environment, where muscle and collagen fibers coexist. A limitation of previous *in vitro* strategies for evaluating synthetic materials for muscle repair is their focus on a single-cell type when evaluating the mesh materials. Many studies concerned with

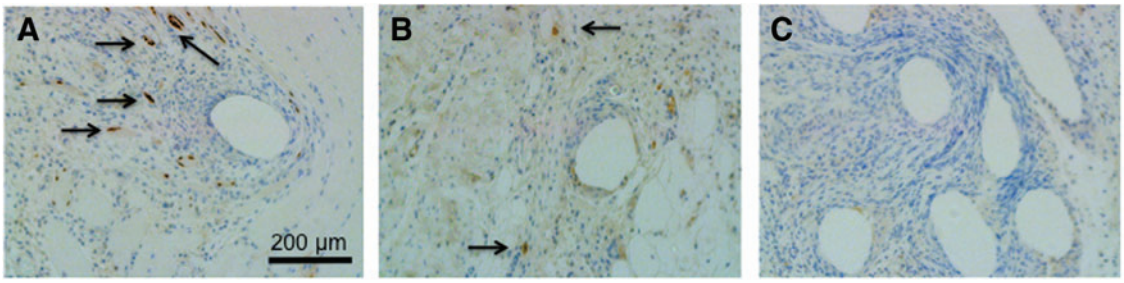

FIG. 8. Immunolabeling of monoclonal mouse anti-myogenin of **(A)** Ch-PPM, **(B)** PPM, and **(C)** Col-PPM. Expression of myogenin (dark brown regions) is limited to cells of skeletal muscle origin and indicates early stages of muscle growth. Qualitatively higher amounts of positive stain of myogenin are seen in Ch-PPM (arrows). All images taken at 10×magnification. Color images available online at www.liebertpub.com/tea

muscle cell attachment on mesh scaffolds seeded solely fibroblasts or solely myoblasts on the mesh.[24–26] We believe that a coculture of primary cultures of myoblasts and fibroblasts provides better evidence of how a mesh will perform *in vivo*. Preferential promotion of the attachment of myoblasts as opposed to fibroblasts in the coculture environment may provide a better predictive metric to evaluate synthetic mesh materials *in vitro*.

The *in vitro* results that show the chitosan coating on polypropylene promotes myoblast early attachment over fibroblast attachment are further supported by *in vivo* observation that Ch-PPM generates significantly higher tetanic force, indicating the ingrowth of muscle fibers. The exact underlying mechanism of the effect is not clear. Diegelmann *et al.* postulate that one possible explanation may be related to the microenvironment in response to chitosan.[27] In their study, fibroblasts that appeared in the chitosan-treated polyvinyl alcohol sponges were smaller and more circular compared to the spindle-shaped fibroblasts observed in the control wounds. It is possible that chitosan may slow the attachment of fibroblasts. The SEM analysis suggests that the microarchitecture of the chitosan polypropylene offers a greater surface area for cell attachment and smaller pores for cell entrapment when compared to the reference mesh, which is supported by our observation that cells were observed atop the chitosan coating in our *in vitro* portion of the study. The polypropylene serves as the skeleton and reinforced structure for the cells, and the microporous architecture of the chitosan sponge allows for easy cell attachment atop the interstices of the polypropylene knitted mesh. We believe that the higher force generation seen in the neo-tissue associated with the Ch-PPM group is due to functional muscle tissue ingrowth. As opposed to fibrotic tissue, functional muscle tissue will respond to electric stimulation to generate force. Both force generation and assessment of myogenin expression confirm the ingrowth of muscle tissue in Ch-PPM. Other tissue integration will not cause such an enhancement. Additional studies are needed to understand how the number and arrangement of muscle fibers relate to *in situ* force generation observations.

Chitosan scaffolds induce only a minimal inflammatory reaction in a rat model. Although the material recruits neutrophils to the site of implantation, the neutrophils are not activated and the material induces neither lymphocyte proliferation nor antibody responses.[28] Histopathological assessment of Ch-PPM implants in the present study found a moderate accumulation of primarily macrophages and fewer multinucleated giant cells at the implant–tissue interface that was unchanged from 2 to 12 weeks postimplantation. In contrast, the tissue reaction to PPM at 12 weeks consisted of a mixed mononuclear cell response that included varying numbers of lymphocytes and plasma cells in addition to macrophages and multinucleated giant cells. Interestingly, at 12 weeks of postimplantation, a large sample of both the PPM and Col-PPM was surrounded by locally extensive areas of dystrophic mineralization, which was not observed around the Ch-PPM. Dystrophic mineralization typically occurs in necrotic or degenerated tissues. Our results suggest that chitosan coating alters the host immune response to the mesh resulting in decreased necrosis and tissue degradation. Further studies to confirm these observations and to elucidate the cellular and molecular mechanisms behind this change are needed.

To investigate the histology further, we conducted analysis of the macrophage phenotype at the mesh interface at 14 days of postimplantation. A number of recent studies have demonstrated that, despite the presence of large numbers of immune cells within the site of implantation at early time points (7–14 days postimplantation), some surgical materials are capable of promoting the formation of functional tissue, whereas others elicit a foreign body reaction and tissue encapsulation. It has been suggested that these divergent outcomes are related to phenotypic differences in the macrophage population. The presence of a predominant population of M1 cells has been associated with poor remodeling outcomes, while M2 phenotype macrophages are associated with more integration and functional outcomes. Our results suggest that although a histologically similar population of predominantly mononuclear cells was observed at 14 days, Ch-PPM samples elicit a decreased M1 and increased M2 phenotype as compared to PPM and Col-PPM samples. These results are consistent with recent studies showing improved outcomes associated with materials that elicit an increased M2 response.[8,29–31] These results coupled with the assessment of myogenin expression and the outcomes of the force generation testing favor Ch-PPM over commercially available meshes. The mechanisms by which chitosan may alter the host immune response remain unclear, but appear to be associated with differences in long-term histologic outcomes.

Acknowledgments

The authors thank Sam LoPresti and Ritu Raman for technical assistance. We are also grateful for the generous donation of mesh samples by C.R. Bard, Inc., Covington, GA. The authors would also like to acknowledge the facilities and services provided by the Nanobiotechnology Center (NBTC), the Cornell Center for Materials Research (CCMR), and the Microscopy and Imaging Facility, Life Sciences Core Laboratories Center at Cornell University. Natasha Udpa is funded by the NSF Graduate Fellowship Research Program.

Disclosure Statement

No competing financial interests exist.

References

1. Cakmak, A., Cirpanli, Y., Bilensoy, E., Yorganci, K., Caliş, S., Saribaş, Z., *et al.* Antibacterial activity of triclosan chitosan coated graft on hernia graft infection model. Int J Pharm **381,** 214, 2009.
2. Cassar, K., and Munro, A. Surgical treatment of incisional hernia. Br J Surg **89,** 534, 2002.
3. Olsen, A.L., Smith, V.J., Bergstrom, J.O., Colling, J.C., and Clark. A.L. Epidemiology of surgically managed pelvic organ prolapse and urinary incontinence. Obstet Gynecol **89,** 501, 1997.
4. Paulo, N.M., De Brito e Silva, M.S., Moraes, A.M., Rodrigues, A.P., De Menezes, L.B., Miguel, M.P., *et al.* Use of chitosan membrane associated with polypropylene mesh to prevent peritoneal adhesion in rats. J Biomed Mater Res Part B Appl Biomate **91,** 221, 2009.
5. Patel, H., Ostergard, D.R., and Sternschuss, G. Polypropylene mesh and the host response. Int Urogynecol J **23,** 669, 2012.

6. Pierce, L.M., Grunlan, M.A., Hou, Y., Baumann, S.S., Kuehl, T.J., and Muir, T.W. Biomechanical properties of synthetic and biologic graft materials following long-term implantation in the rabbit abdomen and vagina. Am J Obstet Gynecol **200,** 549.e1, 2009.
7. Ayubi, F.S., Armstrong, P.J., Mattia, M.S., and Parker, D.M. Abdominal wall hernia repair: a comparison of Permacol and Surgisis grafts in a rat hernia model. Hernia **12,** 373, 2008.
8. Brown, B.N., Londono, R., Tottey, S., Zhang, L., Kukla, K.A., Wolf, M.T., *et al.* Macrophage phenotype as a predictor of constructive remodeling following the implantation of biologically derived surgical mesh materials. Acta Biomater **8,** 978, 2012.
9. Kilic, D., Agalar, C., Ozturk, E., Denkbas, E.B., Cime, A., and Agalar, F. Antimicrobial activity of cefazolin-impregnated mesh grafts. ANZ J Surg **77,** 256, 2007.
10. Cosson, M., Debodinance, P., Boukerrou, M., Chauvet, M., Lobry, P., Crepin, G., *et al.* Mechanical properties of synthetic implants used in the repair of prolapse and urinary incontinence in women: which is the ideal material? Int Urogynecol J **14,** 169, 2003.
11. Kohli, N., and Miklos, J.R. Use of synthetic mesh and donor grafts in gynecologic surgery. Curr Womens Health Rep **1,** 53, 2001.
12. Sanders, D.L., and Kingsnorth, A.N. Prosthetic mesh materials used in hernia surgery. Expert Rev Med Devices **9,** 159, 2012.
13. Kim, I.-Y., Seo, S.-J., Moon, H.-S., Yoo, M.-K., Park, I.-Y., Kim, B.-C., *et al.* Chitosan and its derivatives for tissue engineering applications. Biotechnol Adv **26,** 1, 2008.
14. Gobin, A.S., Butler, C.E., and Mathur, A.B. Repair and regeneration of the abdominal wall musculofascial defect using silk fibroin-chitosan blend. Tissue Eng **12,** 3383, 2006.
15. Altınel, Y., Öztürk, E., Özkaya, G., Akyıldız, E.Ü., Ulcay, Y., and Özgüç, H. The effect of a chitosan coating on the adhesive potential and tensile strength of polypropylene meshes. Hernia **16,** 709, 2012.
16. Wang, X. A comparison of chitosan and collagen sponges as hemostatic dressings. J Bioact Compat Polym **21,** 39, 2006.
17. Ławniczak, P., Grobelski, B., and Pasieka, Z. Properties comparison of intraperitoneal hernia meshes in reconstruction of the abdominal wall: animal model study. Pol Przegl Chir **83,** 19, 2011.
18. Valentin, J.E., Turner, N.J., Gilbert, T.W., and Badylak, S.F. Functional skeletal muscle formation with a biologic scaffold. Biomaterials **31,** 7475, 2010.
19. Snowden, J. Preparing Primary Cultures from Muscle Biopsy Specimens [Internet]. University of Rochester Medical Center Website. p. 5–7, [cited 2010 Aug 11]. Available www.urmc.rochester.edu/fields-center/protocols/myoblast-cell-cultures.cfm.
20. Tsai, W., Chu, C., Chiu, S., and Yao, J. *In vitro* quantitative study of newly made antibacterial braided nylon sutures. Surg Gynecol Obstet **165,** 207, 1987.
21. Sewell, W., Wiland, J., and Craver, B. A new method of comparing sutures of ovine catgut with sutures of bovine catgut in three species. Surg Gynecol Obstet **100,** 483, 1955.
22. Wright, W.E., Sassoon, D.A., and Lin, V.K. Myogenin, a factor regulating myogenesis, has a domain homologous to MyoD. Cell **56,** 607, 1989.
23. Voyles, C.R., Richardson, J.D., Bland, K.I., Tobin, G.R., Flint, L.M., and Polk, H.C. Emergency abdominal wall reconstruction with polypropylene mesh: short-term benefits versus long-term complications. Ann Surg **194,** 219, 1981.
24. Neumann, T., Hauschka, S.D., and Sanders, J.E. Tissue engineering of skeletal muscle using polymer fiber arrays. Tissue Eng **9,** 995, 2003.
25. Hill, E., Boontheekul, T., and Mooney, D.J. Designing scaffolds to enhance transplanted myoblast survival and migration. Tissue Eng **12,** 1295, 2006.
26. Chen, G., Sato, T., Ohgushi, H., Ushida, T., Tateishi, T., and Tanaka, J. Culturing of skin fibroblasts in a thin PLGA-collagen hybrid mesh. Biomaterials **26,** 2559, 2005.
27. Diegelmann, R.F., Dunn, J.D., Lindblad, W.J., and Cohen, I.K. Analysis of the effects of chitosan on inflammation, angiogenesis, fibroplasia, and collagen deposition in polyvinyl alcohol sponge implants in rat wounds. Wound Repair Regen **4,** 48, 1996.
28. VandeVord, P., Matthew, H., DeSilva, S., Mayton, L., Wu, B., and Wooley, P. Evaluation of the biocompatibility of a chitosan scaffold in mice. J Biomed Mater Res **59,** 585, 2002.
29. Mokarram, N., Merchant, A., Mukhatyar, V., Patel, G., and Bellamkonda, R.V. Effect of modulating macrophage phenotype on peripheral nerve repair. Biomaterials **33,** 8793, 2012.
30. Rao, A.J., Gibon, E., Ma, T., Yao, Z., Smith, R.L., and Goodman, S.B. Revision joint replacement, wear particles, and macrophage polarization. Acta Biomater **8,** 2815, 2012.
31. Madden, L.R., Mortisen, D.J., Sussman, E.M., Dupras, S.K., Fugate, J.A., Cuy, J.L., *et al.* Proangiogenic scaffolds as functional templates for cardiac tissue engineering. Proc Natl Acad Sci U S A **107,** 15211, 2010.

Address correspondence to:
Yingxin Gao, PhD
Sibley School of Mechanical and Aerospace Engineering
Cornell University
220 Upson Hall
Ithaca, NY 14850

E-mail: yg75@cornell.edu

Received: December 13, 2012
Accepted: July 3, 2013
Online Publication Date: August 21, 2013